# Electronic state-lifetime interference in the hard x-ray regime: argon as a showcase

G. Goldsztejn,[1,*] R. Püttner,[2] L. Journel,[1,3] R. Guillemin,[1,3] O. Travnikova,[1,3] R. K. Kushawaha,[1] B. Cunha de Miranda,[1] I. Ismail,[1] D. Céolin,[3] M. N. Piancastelli,[1,4] M. Simon,[1,3] and T. Marchenko[1,3,†]

[1]*Sorbonne Universités, UPMC Univ Paris 06, CNRS, UMR 7614, Laboratoire de Chimie Physique-Matière et Rayonnement, F-75005, Paris, France*

[2]*Institut für Experimentalphysik, Freie Universität Berlin, Arnimallee 14, D-14195 Berlin, Germany*

[3]*Synchrotron SOLEIL, l'Orme des Merisiers, Saint-Aubin, BP 48, F-91192 Gif-sur-Yvette Cedex, France*

[4]*Department of Physics and Astronomy, Uppsala University, PO Box 516, SE-751 20 Uppsala, Sweden*

(Dated: January 6, 2017)

Electronic state-lifetime interference is a phenomenon specific for ionization of atoms and molecules in the hard x-ray regime. Using resonant $KL_{2,3}L_{2,3}$ Auger decay in argon as a showcase, we present a model that allows extracting the interference terms directly from the cross sections of the final electronic states. The analysis provides fundamental information on the excitation and decay processes such as probabilities of various decay paths and the values of the dipole matrix elements for transitions to the excited states. Our results shed light on the interplay between spectator, shake-down and shake-up processes in the relaxation of deep core-hole states.

PACS numbers: 33.80.Eh, 34.50.Gb

## I. INTRODUCTION

Interference is a key phenomenon in quantum physics, more particularly so in the interaction of light with matter. From Young's experiment [1] to quantum optics experiments where only one photon is emitted [2–4], the observed interference patterns demonstrated that systems could be prepared in a coherent superposition of states. In atomic and molecular physics, interference effects can occur if different excited electronic and/or vibrational states are coherently populated and decay into the same final state.

As an example, coherent excitation of different vibrational states with the natural lifetime broadening of the same order of magnitude as the vibrational spacing, leads to the lifetime-vibrational interference (LVI) phenomenon. This has been thoroughly studied in the soft x-ray regime, where several experiments on the CO molecule at the C $1s \rightarrow \pi^*$ resonance [5–9], at the C $1s \rightarrow$ Rydberg orbitals [10] and at the O $1s \rightarrow \pi^*$ resonance [11] showed evidence of the LVI effects. Later such effects were also observed in the $N_2$ [12] and $O_2$ [13] molecules.

In the hard x-ray regime, the lifetime broadening of excited states can be on the order of 1 eV, that is comparable to the energy spacing between the excited electronic states. Different excited states can therefore be coherently populated and can decay, either through spectator Auger or with involvement of shake processes, into the same final state, which induces electronic state-lifetime interference (ELI).

Interference phenomena between discrete and continuum electronic states were predicted by Fano long time ago [14]. Åberg developed a unified theory that takes into account LVI and ELI effects [15] and Cesar *et al.* elaborated a theoretical description of these phenomena in the case of radiative and non-radiative decays [16]. However, only few experimental observations of ELI can be found in literature. Levin *et al.* performed coincidence measurements between ions and Auger electrons at the $K$-edge of the argon atom [17], Rubensson *et al.* observed interference effects between the $1s^{-1}3p'$ and $1s^{-1}4p'$ resonances in the neon atom [18]. LeBrun *et al.* measured Auger spectra after resonant excitation or ionization at the $K$-edge in argon with an experimental resolution above 1 eV and observed an asymmetric profile in the $2p^{-2}5p^{+}$ cross section due to ELI [19]. Here and in the following, we use the notation $np'$ for the excited electronic states and $np^{+}$ for the final ionized states to avoid confusion. In all the studies cited above, a modest experimental resolution did not allow the authors to disentangle the contributions of different intermediate states relaxing into one particular final state.

Lately, high-resolution resonant inelastic x-ray scattering measurements allowed observation of ELI in the core-excited HCl molecule [20]. However, due to strict selection rules governing the radiative decay, the observed ELI effect was rather weak. Recently, the high-resolution hard x-ray photoemission spectroscopy (HAXPES) end-station installed on the GALAXIES beamline at the French synchrotron SOLEIL, enabled us to observe strong ELI effects in resonant Auger spectra at the $K$-edge in argon [21], at the $L$-edge in xenon [22], and at the Cl $K$-edge in the HCl and $CH_3Cl$ molecules [23]. The ELI has been observed in the cross sections of the final states reflecting the direct contributions of different decay channels as well as the interference occurring between those.

In [23] we introduced a model that allows extracting the ELI terms as well as the intensity ratios of the overlapping final states. In the present paper, we demonstrate the capacity of this model to provide fundamental

*Present adress: gildas.goldsztejn@mbi-berlin.de

†E-mail: tatiana.marchenko@upmc.fr

information on the excitation and decay processes such as probabilities of different decay channels and the values of the dipole transition matrix elements for the excitation at the $K$-edge in the argon atom. The article is organized as follows: the experimental set-up is described in section II, the model formalism is detailed in section III, we present our data analysis and results in section IV and give our conclusions in section V.

## II. EXPERIMENTAL DETAILS

The experimental set-up was thoroughly described in [24]. Briefly, the measurements were performed using the end-station HAXPES, based on a hemispherical electron analyzer permanently installed on the GALAXIES beamline at the synchrotron SOLEIL [25]. The analyzer has a wide angular acceptance and allows measurements of high-energy electrons (up to 10 keV) that can be emitted from atoms and molecules ionized with the photons of the GALAXIES beamline in the 2.3-12 keV energy range. The X-ray light from the U20 undulator is linearly polarized in the horizontal plane and monochromatized by a Si(111) double-crystal monochromator. The lenses of the analyzer are set parallel to the polarization vector. Note that due to the fixed experimental geometry, the cross sections discussed throughout the paper are not the absolute cross sections (see [22, 23, 26] for details). The total instrumental resolution of 460 meV [21] includes the contributions of the photon bandwidth ($\approx$ 400 meV), the spectrometer resolution ($\approx$ 200 meV) and the thermal Doppler broadening ($\approx$ 100 meV), since the measurements were performed at room temperature. The $KL_{2,3}L_{2,3}$ Auger spectra were recorded while changing the incident photon energy across the $1s - np'$ ($n \geq 4$) resonances and up to 1 eV above ionization threshold.

In order to extract the cross sections of the final states as a function of the incident photon energy, we follow the procedure described in [21]. The peaks in the Auger spectra corresponding to the $2p^{-2}np^{+}$ ($n \geq 4$) final states were fitted with Voigt functions, which represent a convolution between a Lorentzian function describing the electronic transition to the final state and a Gaussian function taking into account the total instrumental resolution.

## III. SIMULATIONS

In our recent work [23] we have developed a model allowing to qualitatively describe the effect of ELI in the cross sections of the final states in the Auger spectra of core-excited atoms and molecules. In general, the model describes the interference between multiple excited electronic states as well as takes into account nuclear dynamics occurring in a dissociative excited molecular state. Here, we demonstrate that in the case of argon atom the model allows extracting quantitative information about the dipole transition matrix elements for the Ar $1s$ excitation and the probabilities of different decay channels. For clarity, here we outline the formalism of the model in a basic case of two discrete electronic excited states.

The cross section $\sigma(\omega)$ of a given final state is described by the Kramers-Heisenberg formula [27]:

$$\sigma(\omega) \propto \left| \sum_c \frac{\langle \Phi_f | \boldsymbol{\mathcal{Q}} | \Phi_c \rangle \langle \Phi_c | \boldsymbol{\mathcal{D}} | \Phi_o \rangle}{\omega - \tau_c + i\Gamma_c/2} \right|^2 \delta(\omega - \omega' - \tau_f, \Gamma_c), \tag{1}$$

where $\sum_c$ represents the sum over all the intermediate electronic states, $\langle \Phi_c | \boldsymbol{\mathcal{D}} | \Phi_o \rangle$ is the dipole matrix element that corresponds to the transition from the ground state described by the wavefunction $\Phi_o$ to the intermediate excited state described by the wavefunction $\Phi_c$, and $\langle \Phi_f | \boldsymbol{\mathcal{Q}} | \Phi_c \rangle$ is the Coulombian matrix element corresponding to the transition from the intermediate to the final state described by the wavefunction $\Phi_f$. Further, $\omega$ and $\omega'$ are, respectively, the energies of the incident photon and of the emitted Auger electron, $\tau_c$ and $\tau_f$ are the energy differences between the ground and the intermediate electronic states, and between the ground and the final electronic states, respectively, $\Gamma_c$ is the lifetime broadening of the intermediate state. Finally $\delta(\omega - \omega' - \tau_f, \Gamma_c)$ is a Lorentzian function that takes into account the energy conservation throughout the whole absorption/decay process.

In the case of two discrete intermediate electronic states, the cross section can be rewritten:

$$\sigma(\omega) \propto \left| \frac{K_1}{\omega - \tau_1 + i\Gamma_1/2} + \frac{K_2}{\omega - \tau_2 + i\Gamma_2/2} \right|^2, \tag{2}$$

where $K_c = \langle \Phi_f | \boldsymbol{\mathcal{Q}} | \Phi_c \rangle \langle \Phi_c | \boldsymbol{\mathcal{D}} | \Phi_o \rangle$ ($c$ =1 or 2). The right side of Eqn.2 can be developed into a sum of two Lorentzian functions and a cross term:

$$\begin{aligned} \sigma(\omega) \;\propto\; & Lor(\Gamma_1, \tau_1, K_1, \omega) + Lor(\Gamma_2, \tau_2, K_2, \omega) \\ & + \frac{(K_1 K_2^* + K_1^* K_2) \cdot ((\omega - \tau_1)(\omega - \tau_2) + \frac{\Gamma_1 \cdot \Gamma_2}{4})}{\left[(\omega - \tau_1)^2 + \frac{\Gamma_1^2}{4})\right] \left[(\omega - \tau_2)^2 + \frac{\Gamma_2^2}{4})\right]}. \end{aligned} \tag{3}$$

In the case of $KLL$ Auger decay, the core holes created in both the intermediate and the final states can be considered as sufficiently deep to remain unaffected by the presence of an excited electron in a valence shell. This allowed Armen *et al.* [28] to make an approximation suggesting that the Coulombian matrix element can be decomposed into a constant partial $KLL$ Auger rate amplitude and an overlap integral:

$$\langle 1s^{-1} mp' | \boldsymbol{\mathcal{Q}} | 2p^{-2} np^{+} \rangle = \langle 1s^{-1} | \boldsymbol{\mathcal{Q}} | 2p^{-2} \rangle \langle mp' | np^{+} \rangle. \tag{4}$$

Here $\Gamma_{KLL} = \left| \langle 1s^{-1} | \boldsymbol{\mathcal{Q}} | 2p^{-2} \rangle \right|^2$ is the partial Auger rate for the $KLL$ transition, and $\left| \langle mp' | np^{+} \rangle \right|^2$ is directly related to the probability of spectator or shake processes.

After introducing Eqn. 4 into Eqn. 3, we obtain:

$$\sigma(\omega) \propto Lor(\Gamma_1,\tau_1,k_1,\omega)+Lor(\Gamma_2,\tau_2,k_2,\omega) + \frac{(k_1k_2^*+k_1^*k_2)\cdot((\omega-\tau_1)(\omega-\tau_2)+\frac{\Gamma_1\cdot\Gamma_2}{4})}{\left[(\omega-\tau_1)^2+\frac{\Gamma_1^2}{4})\right]\left[(\omega-\tau_2)^2+\frac{\Gamma_2^2}{4})\right]}. \quad (5)$$

Here $k_{1,2}=\frac{K_{1,2}}{\sqrt{\Gamma_{KLL}}}=\langle 1s^{-1}mp'|\boldsymbol{\mathcal{D}}|\Phi_0\rangle\langle mp'|np^+\rangle$. Note that $K_{1,2}$ and $k_{1,2}$ can be chosen as real parameters without loss of generality [23], then $k_1k_2^*+k_1^*k_2=2k_1k_2$.

In the following we will apply Eqn.5 for fitting the experimental cross-sections of the final states $2p^{-2}np^+$, using $k_{1,2}$, $\tau_{1,2}$ and $\Gamma_{1,2}$ as fit parameters. Analysis of the fitting results allows obtaining quantitative estimates for the excitation dipole transition matrix elements and for the probabilities of different decay channels. The results of our analysis are presented in the following section.

## IV. RESULTS

Figure 1 presents the results of fitting the experimental cross sections of the final states $2p^{-2}np^+$ $(4\le n\le 7)$ plotted as a function of the photon energy relative to the ionization potential (IP). Here the dots are the experimental points and the lines are the results of our fits. We assumed the lifetime broadening $\Gamma$ to be constant for all core-excited states $1s^{-1}mp'$. The fitting provides the value $\Gamma=0.7$ eV, in agreement with [29]. The cross sections of the final states $2p^{-2}4p^+$, $2p^{-2}5p^+$, $2p^{-2}6p^+$ and $2p^{-2}7p^+$ are normalized to the dominant peak intensities: $I_{4p}=4593.5$, $I_{5p}=1546.2$, $I_{6p}=1119.1$ and $I_{7p}=646.4$, respectively. The intensity values are in arbitrary units and are related to the statistics of our experimental conditions, such as gas pressure, acquisition time etc.

The energies $E_{m,l}$ of the resonantly excited intermediate states $1s^{-1}mp'$ $(4\le m\le 9)$, are indicated with vertical lines in Fig.1 and summarized in Table I. The energy value of the $1s^{-1}4p'$ state was determined from the fit of the $2p^{-2}4p^+$ cross section, while keeping free the $\tau_c$ fitting parameter describing the energy of the resonant transition from the ground to the intermediate state (see Eqns. 1 and 5). The determined energy of the $1s^{-1}4p'$ state and the known value of the IP (3205.9 eV) allowed calculating the quantum defect ($\delta=1.72$) and, therefore, empirically determine the resonant energies of the other $1s^{-1}mp'$ states:

$$E_{m,l}=IP-\frac{Ry}{(m-\delta)^2} \quad (6)$$

where $Ry$ is the Rydberg constant.

The cross section of the $2p^{-2}4p^+$ final state shown in Fig. 1, contains one broad peak with the maximum located close to the resonant energy of the $1s-4p$ transition, which reflects the dominance of the spectator Auger decay. The absence of any significant asymmetry or shift

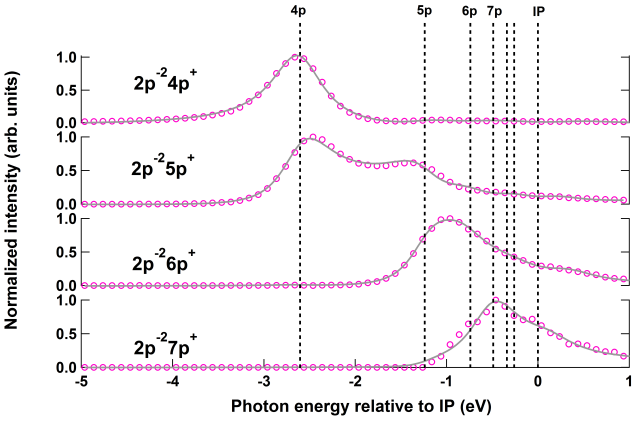


FIG. 1: The cross sections of the final states $2p^{-2}np^+$ $(4\le n\le 7)$ plotted as a function of the photon energy relative to the ionization potential. The dots are the experimental points and the lines are the fitting results. The vertical lines indicate the energies of the resonantly excited intermediate states $1s^{-1}mp'$ $(4\le m\le 9)$.

| Electronic state | $E_{m,l}$ (eV) |
|---|---|
| $1s^{-1}4p'$ | -2.61 |
| $1s^{-1}5p'$ | -1.24 |
| $1s^{-1}6p'$ | -0.74 |
| $1s^{-1}7p'$ | -0.49 |
| $1s^{-1}8p'$ | -0.34 |
| $1s^{-1}9p'$ | -0.26 |

TABLE I: The energies of the resonantly excited intermediate states $1s^{-1}mp'$ $(4\le m\le 9)$, relative to the IP.

from the resonant $1s^{-1}4p'$ excitation energy, indicates the weakness of the ELI effects in this case.

A very different situation can be observed in the cross section of the $2p^{-2}5p^+$ final state dominated by two intense peaks. One peak is located close to the $1s^{-1}5p'$ resonance and corresponds to the spectator Auger decay. The other peak has the maximum near the energy of the $1s-4p$ transition and corresponds to a shake-up process, where the excited electron, initially promoted to the $4p$ orbital, ends up in the $5p$ orbital in the final state. One can observe that both peaks are strongly asymmetric and their maxima are displaced with respect to the resonant energies, which indicates a strong manifestation of the ELI phenomenon. The reduction of the energy difference between the maxima of the peaks, observed in the cross section of the $2p^{-2}5p^+$ final state, with respect to the difference between the resonant energies of the $1s-4p$ and $1s-5p$ transitions, is characteristic for the manifestation of ELI between the spectator Auger decay and the decay channel with involvement of a shake-up process [23, 30]. Furthermore, a weak contribution near the energy of the $1s-6p$ transition in the cross section of the $2p^{-2}5p^+$ final state, corresponds to a shake-down process, where the excited electron, initially promoted to the $6p$ orbital,

ends up in the $5p$ orbital in the final state.

The cross section of the $2p^{-2}6p^{+}$ final state contains a broad, asymmetric peak located between the $1s^{-1}5p'$ and $1s^{-1}6p'$ resonances and a shoulder near the $1s^{-1}7p'$ resonance. A detailed analysis of various decay channels contributing to this cross section and the role of the ELI effects are presented below (see figure 2).

Finally, in the cross section of the $2p^{-2}7p^{+}$ final state, one can observe a dominant peak located near the $1s^{-1}7p'$ resonance, corresponding to the spectator decay, and several shoulders at lower and higher energies due to contributions from shake-up and shake-down processes, respectively.

The relative amplitudes of different decay channels contributing to each of the final states have been obtained as a result of our fitting procedure using Eqn.5. The corresponding fit parameters $k = \langle\Phi_0|\boldsymbol{\mathcal{D}}|1s^{-1}mp'\rangle\langle mp'|np^{+}\rangle$ are summarized in Table II, where the relative amplitudes are normalized to the peak intensity of the dominant contribution $\mathrm{I}_{np}$ $(4 \leq n \leq 7)$ as described above in relation to Figure 1. Analysis of the results presented in Table II allows us to make two observations.

First, one can observe that the amplitudes of the decay channels involving shake-up processes have a sign opposite to that of the spectator decay channels and the decays accompanied by shake-down processes. Although the physical interpretation requires further theoretical analysis, we assume that this observation may be related to the difference in the size of the orbitals occupied by the excited electron in the intermediate and the final states.

The observed trend is directly related to the relative displacements of the peaks in the cross sections of the final states due to the ELI effect. The direction of the relative displacement depends on the sign of the interference cross-term in Eqn.5, which is determined by the product $k_1k_2$ of the relative amplitudes of the interfering decay channels. As demonstrated in figure 1, the maxima of the peaks corresponding to the spectator Auger decay and the decay channel with involvement of a shake-up process are displaced towards each other due to the ELI effect. In this case the product of the relative amplitudes of the interfering channels and, hence, the interference cross-term have a negative sign. One can show that in the case of interfering spectator decay and the decay channel involving a shake-down process, the interference cross-term is positive and the maxima of the peaks are shifted away from each other.

A second observation resulting from the analysis of Table II indicates the dominance of the decay channel accompanied by a shake-up process in the cross-sections of the $2p^{-2}5p^{+}$ and the $2p^{-2}6p^{+}$ final states. This effect may be related to the contraction of the Rydberg orbitals upon the $KLL$ Auger decay. Namely, the Auger decay leads to a sudden enhancement of the effective charge seen by the electrons in the outer orbitals, causing the orbitals contraction towards the nucleus. In this case, an overlap between the intermediate $1s^{-1}5p'$ and the final $2p^{-2}6p^{+}$ states may become larger than an overlap between the intermediate $1s^{-1}6p'$ and the final $2p^{-2}6p^{+}$ states, thus favoring decay through a shake-up process over the spectator decay.

| Final state | Fit parameter $k$ | Decay type |
|---|---|---|
| $2p^{-2}4p^{+}$ | $\langle\Phi_0\|\boldsymbol{\mathcal{D}}\|1s^{-1}4p'\rangle\langle 4p'\|4p^{+}\rangle$ = 1.00 | spectator |
| | $\langle\Phi_0\|\boldsymbol{\mathcal{D}}\|1s^{-1}5p'\rangle\langle 5p'\|4p^{+}\rangle$ = 0.15 ± 0.01 | shake-down |
| | $\langle\Phi_0\|\boldsymbol{\mathcal{D}}\|1s^{-1}6p'\rangle\langle 6p'\|4p^{+}\rangle$ = 0.07 ± 0.03 | shake-down |
| | $\langle\Phi_0\|\boldsymbol{\mathcal{D}}\|1s^{-1}7p'\rangle\langle 7p'\|4p^{+}\rangle$ = 0.04 ± 0.03 | shake-down |
| $2p^{-2}5p^{+}$ | $\langle\Phi_0\|\boldsymbol{\mathcal{D}}\|1s^{-1}4p'\rangle\langle 4p'\|5p^{+}\rangle$ = -1.00 | shake-up |
| | $\langle\Phi_0\|\boldsymbol{\mathcal{D}}\|1s^{-1}5p'\rangle\langle 5p'\|5p^{+}\rangle$ = 0.49 ± 0.02 | spectator |
| | $\langle\Phi_0\|\boldsymbol{\mathcal{D}}\|1s^{-1}6p'\rangle\langle 6p'\|5p^{+}\rangle$ = 0.22 ± 0.04 | shake-down |
| | $\langle\Phi_0\|\boldsymbol{\mathcal{D}}\|1s^{-1}7p'\rangle\langle 7p'\|5p^{+}\rangle$ = 0.15 ± 0.10 | shake-down |
| $2p^{-2}6p^{+}$ | $\langle\Phi_0\|\boldsymbol{\mathcal{D}}\|1s^{-1}4p'\rangle\langle 4p'\|6p^{+}\rangle$ = -0.10 ± 0.03 | shake-up |
| | $\langle\Phi_0\|\boldsymbol{\mathcal{D}}\|1s^{-1}5p'\rangle\langle 5p'\|6p^{+}\rangle$ = -1.00 | shake-up |
| | $\langle\Phi_0\|\boldsymbol{\mathcal{D}}\|1s^{-1}6p'\rangle\langle 6p'\|6p^{+}\rangle$ = 0.57 ± 0.04 | spectator |
| | $\langle\Phi_0\|\boldsymbol{\mathcal{D}}\|1s^{-1}7p'\rangle\langle 7p'\|6p^{+}\rangle$ = 0.32 ± 0.04 | shake-down |
| $2p^{-2}7p^{+}$ | $\langle\Phi_0\|\boldsymbol{\mathcal{D}}\|1s^{-1}4p'\rangle\langle 4p'\|7p^{+}\rangle$ = 0.00 | shake-up |
| | $\langle\Phi_0\|\boldsymbol{\mathcal{D}}\|1s^{-1}5p'\rangle\langle 5p'\|7p^{+}\rangle$ = -0.31 ± 0.08 | shake-up |
| | $\langle\Phi_0\|\boldsymbol{\mathcal{D}}\|1s^{-1}6p'\rangle\langle 6p'\|7p^{+}\rangle$ = -0.15 ± 0.11 | shake-up |
| | $\langle\Phi_0\|\boldsymbol{\mathcal{D}}\|1s^{-1}7p'\rangle\langle 7p'\|7p^{+}\rangle$ = 1.00 | spectator |

TABLE II: Relative amplitudes of different decay channels contributing to the cross sections of the $2p^{-2}np^{+}$ final states, normalized to the intensity of the dominant peak.

The roles of different decay channels and the influence of the ELI are illustrated in the cross section of the $2p^{-2}6p^{+}$ final state presented in Fig. 2. The dominant contribution is the decay channel involving a shake-up process, where the excited electron, initially promoted to the $5p$ orbital, results in the $6p$ orbital in the final state. A strong interference between the spectator decay (thin solid blue line) and the decay involving a shake-up process (thick dashed red line) becomes evident through a corresponding interference cross-term (thick dash-dotted red line). Due to the negative sign of the cross-term, the peaks of the interfering contributions shift towards each other, merging into a single broad asymmetric peak in the cross section of the final state (thick solid grey line) with a maximum located at the relative energy around -1 eV, between the $1s^{-1}5p'$ and $1s^{-1}6p'$ resonances (see Table I). The contribution of the decay channel involving a shake-down process, where the excited electron, initially promoted to the $7p$ orbital, ends up in the $6p$ orbital in the final state, is relatively weak (thin dashed green line). However, the interference cross-term between the spectator decay and the decay through a shake-down process is rather intense (thin dash-dotted green line), giving rise to the shoulder in the cross section of the final state at the relative energy of -0.5 eV, near the $1s^{-1}7p'$ resonance. A shoulder observed in the cross section above the IP, is due to interference with the states in the continuum, which is taken into account in our fitting procedure by

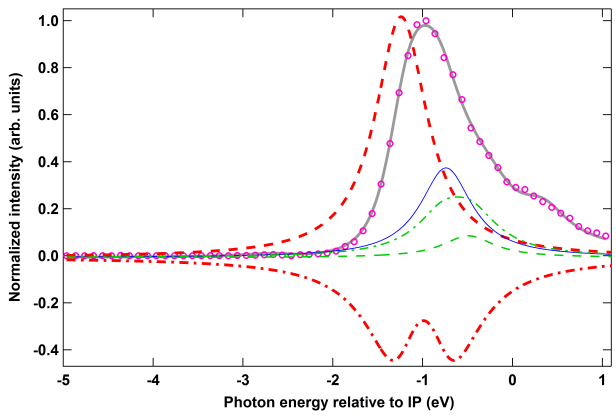


FIG. 2: The cross section of the $2p^{-2}6p^{+}$ final state plotted as a function of the photon energy relative to the ionization potential. The dots are the experimental points, the thick solid grey line is the fitting result. The thin solid blue, thick dashed red and thin dashed green lines show the contributions of the spectator decay, the decay accompanied by a shake-up process from the $5p$ orbital, and the decay involving a shake-down process from the $7p$ orbital, respectively. The interference cross-terms between the $1s^{-1}6p'$ and $1s^{-1}5p'$ electronic states and between the $1s^{-1}6p'$ and $1s^{-1}7p'$ electronic states are shown with thick dash-dotted red and thin dash-dotted green lines, respectively.

an arctangent function.

The preceding discussion elucidates the relative contributions of different decay channels contributing to a cross section of a given final state. Further analysis allows obtaining relative probabilities of possible decay channels for a given intermediate excited state directly from the fit parameters $k$ summarized in Table II and the peak intensities of the cross sections of the final states $\mathrm{I}_{np}$ $(4 \le n \le 7)$ .

For example, for the intermediate state $1s^{-1}4p'$ decaying predominantly into the $2p^{-2}4p^{+}$ and $2p^{-2}5p^{+}$ final states, we obtain:

$$\frac{\mathrm{I}_{4p}}{\mathrm{I}_{4p}+\mathrm{I}_{5p}}\left|\langle 4p'|4p^{+}\rangle\right|^2+\frac{\mathrm{I}_{5p}}{\mathrm{I}_{4p}+\mathrm{I}_{5p}}\left|\langle 4p'|5p^{+}\rangle\right|^2=1, \text{and} \quad (7)$$

$$\frac{\mathrm{I}_{5p}\left|\langle 1s^{-1}4p'|\boldsymbol{\mathcal{D}}|\Phi_0\rangle\right|^2\left|\langle 4p'|5p^{+}\rangle\right|^2}{\mathrm{I}_{4p}\left|\langle 1s^{-1}4p'|\boldsymbol{\mathcal{D}}|\Phi_0\rangle\right|^2\left|\langle 4p'|4p^{+}\rangle\right|^2}=\alpha^2,$$

$$\frac{\mathrm{I}_{4p}}{\mathrm{I}_{4p}+\mathrm{I}_{5p}}(\alpha^2+1)\left|\langle 4p'|4p^{+}\rangle\right|^2=1.$$

Then the probability of the spectator decay is $\frac{\mathrm{I}_{4p}}{\mathrm{I}_{4p}+\mathrm{I}_{5p}}\left|\langle 4p'|4p^{+}\rangle\right|^2=\frac{1}{1+\alpha^2}$ and the probability of a decay through a shake-up process is $\frac{\mathrm{I}_{5p}}{\mathrm{I}_{4p}+\mathrm{I}_{5p}}\left|\langle 4p'|5p^{+}\rangle\right|^2=1-\frac{1}{1+\alpha^2}$ .

The probabilities of different decay channels for the $1s^{-1}mp'$ $(m=4,5,6)$ intermediate states are shown in Table III. For all intermediate states the decay to the $2p^{-2}np^{+}$ final states with $n \ge 8$ has been neglected due to insufficient statistics of the data. For the same reason the decay of the $1s^{-1}4p'$ intermediate state has been limited by the $2p^{-2}4p^{+}$ and $2p^{-2}5p^{+}$ final states, and the case of the $1s^{-1}7p'$ intermediate state has been omitted. The results presented in Table III show that the decay through a shake process has a substantial probability, comparable to that of the spectator decay and may even occur to be the dominant decay channel as is the case for the $1s^{-1}5p'$ state decaying predominantly through a shake-up process to the $2p^{-2}6p^{+}$ final state.

| Intermediate states | Final states | Decay probability |
|---|---|---|
| $1s^{-1}4p'$ | $2p^{-2}4p^{+}$ | 0.75 |
| | $2p^{-2}5p^{+}$ | 0.25 |
| $1s^{-1}5p'$ | $2p^{-2}4p^{+}$ | 0.06 |
| | $2p^{-2}5p^{+}$ | 0.22 |
| | $2p^{-2}6p^{+}$ | 0.68 |
| | $2p^{-2}7p^{+}$ | 0.04 |
| $1s^{-1}6p'$ | $2p^{-2}4p^{+}$ | 0.05 |
| | $2p^{-2}5p^{+}$ | 0.16 |
| | $2p^{-2}6p^{+}$ | 0.76 |
| | $2p^{-2}7p^{+}$ | 0.03 |

TABLE III: Probabilities of different decay channels for the $1s^{-1}mp'$ $(m=4,5,6)$ intermediate states.

As we have shown, the analysis of our fitting results using Eqn.7 allows extracting the probabilities of different decay channels $\left|\langle mp'|np^{+}\rangle\right|^2$ described by the overlap integrals independently of the dipole matrix elements. Likewise, the intensities of the absorption electronic transitions $\left|\langle\Phi_0|\boldsymbol{\mathcal{D}}|1s^{-1}mp'\rangle\right|^2$ described by the dipole matrix elements can be obtained from the results of our fitting procedure independently of the overlap integrals. For example, for the $1s^{-1}4p'$ intermediate state decaying predominantly into the $2p^{-2}4p^{+}$ and $2p^{-2}5p^{+}$ final states, we obtain from the fit parameters presented in Table II:

$$\frac{\mathrm{I}_{4p}}{\mathrm{I}_{4p}+\mathrm{I}_{5p}}k_{4p}^2+\frac{\mathrm{I}_{5p}}{\mathrm{I}_{4p}+\mathrm{I}_{5p}}k_{5p}^2=\left|\langle 1s^{-1}4p'|\boldsymbol{\mathcal{D}}|\Phi_0\rangle\right|^2\times \quad (8)$$
$$\left(\frac{\mathrm{I}_{4p}\left|\langle 4p'|4p^{+}\rangle\right|^2+\mathrm{I}_{5p}\left|\langle 4p'|5p^{+}\rangle\right|^2}{\mathrm{I}_{4p}+\mathrm{I}_{5p}}\right),$$

where $k_{4p}^2=\left|\langle 1s^{-1}4p'|\boldsymbol{\mathcal{D}}|\Phi_0\rangle\right|^2\left|\langle 4p'|4p^{+}\rangle\right|^2$ and $k_{5p}^2=\left|\langle 1s^{-1}4p'|\boldsymbol{\mathcal{D}}|\Phi_0\rangle\right|^2\left|\langle 4p'|5p^{+}\rangle\right|^2$.

Taking into account Eqn.7 we obtain:

$$\left|\langle 1s^{-1}4p'|\boldsymbol{\mathcal{D}}|\Phi_0\rangle\right|^2=\frac{\mathrm{I}_{4p}}{\mathrm{I}_{4p}+\mathrm{I}_{5p}}k_{4p}^2+\frac{\mathrm{I}_{5p}}{\mathrm{I}_{4p}+\mathrm{I}_{5p}}k_{5p}^2 \quad (9)$$

Alternatively, the dipole matrix elements can be extracted from the fit of the absorption spectrum. However, the major advantage of our method consists in the high resolution measurements provided by the Auger

spectroscopy performed in the Raman regime. This allows identification of the resonantly excited intermediate states summarized in Table I, which cannot be resolved in the absorption spectrum.

Generally, one can use the intensities of the absorption transitions obtained from Eqns.8 and 9 for reconstruction of the absorption spectrum. Since our aforementioned experimental conditions do not allow measurements of the absolute cross sections, the spectrum reconstructed from the dipole matrix elements using Eqns. 8 and 9 represents a partial electron yield (PEY). The reconstructed PEY can be compared to the experimental PEY obtained directly from the measurements by integrating over the electron kinetic energy the Auger spectra recorded for different photon energies.

There is a generally good agreement between the experimental and the reconstructed PEY shown, respectively, in the top and the bottom panels of figure 3. The bars under the reconstructed PEY indicate the intensities $\left|\langle\Phi_0|\boldsymbol{\mathcal{D}}|1s^{-1}mp'\rangle\right|^2$ of the $1s-mp$ absorption transitions ($4 \leq m \leq 7$), extracted from the fitting procedure. One can observe a slight discrepancy between the experimental and the reconstructed PEY beyond the $1s^{-1}7p'$ resonance. This is related to the fact that the intensity of the transition to the $1s^{-1}7p'$ state is overestimated, since it also takes into account the contributions of the transitions to the higher Rydberg states $1s^{-1}mp'$ with $m \geq 8$, which are otherwise neglected in the fitting procedure. The reconstructed PEY shown with a solid line includes the contributions of the transitions to the discrete states as well as the continuum contribution, which has been fitted with an arctangent function for the lack of the experimental data on the 1s ionization cross section.

The reconstructed PEY shown in figure 3 is normalized to the intensity $\left|\langle\Phi_0|\boldsymbol{\mathcal{D}}|1s^{-1}4p'\rangle\right|^2$ of the transition to the $1s^{-1}4p'$ electronic state. The relative intensities of the transitions to the other intermediate states are $0.21\pm0.01$ for the $1s^{-1}5p'$, $0.06\pm0.01$ for the $1s^{-1}6p'$ and $0.1\pm0.01$ for the $1s^{-1}7p'$ electronic states as obtained from the results of our fitting procedure.

## V. CONCLUSIONS

In conclusion, we have demonstrated that in the hard x-ray regime, ELI is a general phenomenon due to large lifetime broadenings of intermediate electronic states. We have shown that for a system with well separated electronic final states, our model developed for the analysis of ELI effects, provides access to the fundamental observables describing excitation and decay of deep core shells. For the excitation process, the model allows extracting the intensities of the absorption transitions to the resonant intermediate states. For the relaxation process, we are able to determine the probabilities of different decay channels including spectator Auger and the decay involving shake-up and shake-down processes. Our results demonstrate a high relevance of the developed model for the interpretation of the Auger electron spectra in the hard x-ray regime, where the data analysis inevitably faces the complexity of the interference phenomenon.

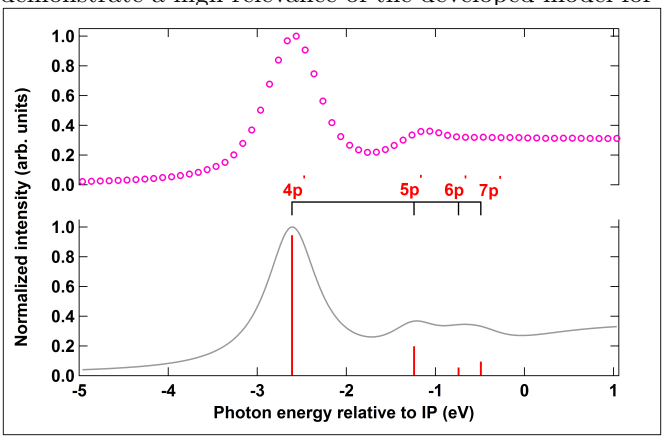


FIG. 3: Experimental (top panel) and reconstructed (bottom panel) PEY. The bars under the reconstructed PEY indicate the intensities of the $1s-mp$ absorption transitions ($4 \leq m \leq 7$), extracted from the fitting procedure, the solid line is the sum of the discrete contributions and the continuum contribution fitted with an arctangent function.

## VI. ACKNOWLEDGEMENTS

Experiments were performed on the GALAXIES beamline at SOLEIL Synchrotron, France (Proposal No. 20120122). We are grateful to D. Prieur for technical assistance and to SOLEIL staff for smoothly running the facility.

[1] T. Young, Phil. Trans. R. Soc. Lond., **92**, 12-48 (1802).
[2] P. Grangier, G. Roger and A. Aspect, Europhys. Lett., **1**, 173 (1986).
[3] P. Grangier and I. Abram, Physics World, **21** (2003).
[4] B. Lounis and M. Orrit, Rep. Prog. Phys., **68**, 1129 (2005).
[5] M. Neeb, J.-E. Rubensson, M. Biermann and W. Eberhardt, J. Electron Spectrosc. Relat. Phenom., **67**, 261 (1994).
[6] S. J. Osborne, A. Ausmees, S. Svensson, A. Kivimäki, O. P. Sairanen, A. Naves de Brito, H. Aksela and S. Aksela, J. Chem. Phys., **102**, 7317 (1995).
[7] M. N. Piancastelli, M. Neeb, A. Kivimäki, B. Kempgens, H. M. Köppe, K. Maier and A. M. Bradshaw, Phys. Rev.

Lett., **77**, 4302 (1996).
[8] S. Sundin, F. K. Gel'mukhanov, H. Ågren, S. J. Osborne, A. Kikas, O. Björneholm, A. Ausmees and S. Svensson, Phys. Rev. Lett., **79**, 1451 (1997).
[9] V. Carravetta, F. K. Gel'mukhanov, H. Ågren, S. Sundin, S. J. Osborne, A. Naves de Brito, O. Björneholm, A. Ausmees and S. Svensson, Phys. Rev. A, **56**, 4665 (1997).
[10] S. Sundin, F. Gel'mukhanov, S. J. Osborne, O. Björneholm, A. Ausmees, A. Kikas, S. L. Sorensen, A. Naves de Brito, R. R. T. Marinho, S. Svensson and H. Ågren, J. Phys. B, **30**, 4267 (1997).
[11] M. N. Piancastelli, M. Neeb, A. Kivimäki, B. Kempgens, H. M. Köppe, K. Maier, A. M. Bradshaw and R. F. Fink, J. Phys. B, **30**, 5677 (1997).
[12] M. N. Piancastelli, A. Kivimäki, B. Kempgens, M. Neeb, K. Maier, U. Hergenhahn, A. Rüdel and A. M. Bradshaw, J. Electron Spectroscop. Relat. Phenom., **98-99**, 111 (1999).
[13] A. Kivimäki, B. Kempgens, M. N. Piancastelli, M. Neeb, K. Maier, A. Rüdel, U. Hergenhahn, A. M. Bradshaw, J. Electron Spectrosc. Relat. Phenom., **93**, 81 (1998).
[14] U. Fano, Phys. Rev., **124**, 1866 (1961).
[15] T. Åberg, Phys. Scripta, **T41**, 71 (1992).
[16] A. Cesar and H. Ågren, Phys. Rev. A, **45**, 2833 (1992).
[17] J. C. Levin, C. Biedermann, N. Keller, L. Liljeby, C.-S. O, R. T. Short, I. A. Sellin and D. W. Lindle, Phys. Rev. Lett., **65**, 988 (1990).
[18] J.-E. Rubensson, M. Neeb, A. Bringer, M. Biermann and W. Eberhardt, Chem. Phys. Lett., **257**, 447 (1996).
[19] T. LeBrun, S. H. Southworth, G. B. Armen, M. A. MacDonald and Y. Azuma, Phys. Rev. A, **60**, 4667 (1999).
[20] M. Kavčič, M. Žitnik, K. Bučar, A. Mihelič, S. Carniato, L. Journel, R. Guillemin and M. Simon, Phys. Rev. Lett., **105**, 113004 (2010).
[21] D. Céolin, T. Marchenko, R. Guillemin, L. Journel, R. K. Kushawaha, S. Carniato, S.-M. Huttula, J.-P. Rueff, G. B. Armen, M. N. Piancastelli and M. Simon, Phys. Rev. A, **91**, 022502 (2015).
[22] R. K. Kushawaha, K. Jänkälä, T. Marchenko, G. Goldsztejn, R. Guillemin, L. Journel, D. Céolin, J.-P. Rueff, A. F. Lago, R. Püttner, M. N. Piancastelli and M. Simon, Phys. Rev. A, **92**, 013427 (2015).
[23] G. Goldsztejn, T. Marchenko, D. Céolin, L. Journel, R. Guillemin, J.-P. Rueff, R. K. Kushawaha, R. Püttner, M. N. Piancastelli and M. Simon, Phys. Chem. Chem. Phys., **18**, 15133 (2016).
[24] D. Céolin, J. M. Ablett, D. Prieur, T. Moreno, J.-P. Rueff, T. Marchenko, L. Journel, R. Guillemin, B. Pilette, T. Marin and M. Simon, J. Electron Spectrosc. Relat. Phenom., **190**, 188 (2013).
[25] J.-P. Rueff, J. M. Ablett, D. Colin, D. Prieur, Th. Moreno, V. Baldent, B. Lassalle, J. E. Rault, M. Simon, and A. Shukla, The GALAXIES Beamline at SOLEIL Synchrotron: Inelastic X-ray Scattering and Photoelectron Spectroscopy in the Hard X-ray Range, J. Synchrotron Rad. 22 (2015), **175**.
[26] G. Goldsztejn, T. Marchenko, R. Püttner, L. Journel, R. Guillemin, S. Carniato, P. Selles, O. Travnikova, D. Céolin, A. F. Lago, R. Feifel, P. Lablanquie, M. N. Piancastelli, F. Penent, M. Simon, Phys. Rev. Lett., **117**, 133001 (2016).
[27] H. A. Kramers and W. Heisenberg, Z. Phys., **31**, 681 (1925).
[28] G. B. Armen, J. C. Levin and I. A. Sellin, Phys. Rev. A **53**, 772 (1996).
[29] J. L. Campbell and T. Papp, At. Data Nucl. Data Tables **77**, 1 (2001).
[30] E. Kukk, H. Aksela, A. Kivimäki, J. Jauhiainen, E. Nõmmiste and S. Aksela, Phys. Rev. A, **56**, 1481 (1997).